Bull Earthquake Eng
DOI 10.1007/s10518-017-0248-x

ORIGINAL RESEARCH PAPER

Experimental observations on the in-plane behaviour of masonry wall infilled RC frames; focusing on deformation limits and backbone curve

Hamood Alwashali[1] · Yuta Torihata[1] · Kiwoong Jin[1] · Masaki Maeda[1]

Received: 17 July 2017 / Accepted: 16 October 2017
© Springer Science+Business Media B.V. 2017

Abstract The ratio of frame strength and stiffness to masonry infill are major parameters that influence the seismic capacity of masonry infill. The influence of such parameters to seismic capacity in terms of strength, stiffness and deformation has significant variations between different design codes and past literature on the topic. This study focused on the in-plane behaviour of unreinforced masonry infill walls installed in reinforced concrete (RC) frames with different strengths. In the first part of this study, two ½ scale specimens with different RC frames and identical masonry infill walls were tested using a static cyclic loading protocol. The main objective was investigating the influence of changing frame strength to seismic capacity in terms of: strength, stiffness and deformation. Results of the presented experiment showed that as the ratio of frame shear strength to masonry shear strength increased, there was great improvement of the masonry infill walls in terms of strength and avoidance of sudden brittle behaviour of the masonry infill. However, varying frame strength did not significantly influence the initial stiffness and story drift at maximum strength. In the second part of this study, an investigation was conducted on the deformation limits of masonry infilled RC frames and the influence of various parameters, based on data collected from many recent experimental tests. Based on these experimental results, the deformation limits of masonry infill were found to be directly proportional to both the compressive prism strength of the masonry infill and the ratio of shear strength of frame to that of the masonry infill. The influence of aspect ratio showed large variation and it is difficult to conclude its level of influence on deformation. A simplified procedure based on experimental data was proposed that can estimate the backbone curve and gave good estimation of the post-peak lateral strength degradation slope based on the ratio of frame strength with simple hand calculation. Such a method is useful in the preliminary design process to help practicing engineers understand the general behaviour expected by infilled RC frames.

✉ Kiwoong Jin
Jin@rcl.archi.tohoku.ac.jp

[1] Graduate School of Engineering, Department of Architectural and Building Science, Tohoku University, Sendai, Japan

Published online: 26 October 2017

Keywords Masonry infill wall · RC moment-resisting frame · Seismic performance evaluation · Static cyclic loading test · Deformation limits

List of symbols

B	Ratio of the boundary frame lateral strength to masonry infill shear strength
V_f	Boundary frame lateral strength
V_{inf}	Masonry infill lateral strength
f_c	Compressive strength of concrete
f_m	Prism compressive strength of masonry infill
t_{inf}	Infill panel thickness
l_{inf}	Infill panel length
M_u	Flexural yield moment of the column or beam
V_{max}	Maximum lateral load of the overall structure (masonry infill and frame)
h_o	Clear height of column
W_{ef}	Equivalent strut width
E_w, E_c	Young's modulus of the infill wall and the concrete
H_{inf}, H	Height of infill wall and the story height
θ	Arctan (H_{inf}/L_{inf}) (the inclination of the diagonal strut)
I_c, I_b	Moment of inertia of the column and of the beam
f_{m90}	Prism compressive strength of masonry in horizontal direction
μ	Coefficient of sliding friction
d_m	Diagonal length of infill panel
h, l	Height and length of frame
R_{crack}	Story drift angle at the cracking point
R_{max}	Story drift angle at maximum strength
R_u	Story drift angle at the strength degradation point is set to be 80% of the maximum strength
K_f	Initial stiffness of frame
K_m	Initial stiffness of masonry infill
K_o	Initial stiffness of whole system (masonry infill and RC frame)
ε_{peak}	Masonry prims compression strain at maximum compression stress
δ_{max}	Lateral displacement at maximum lateral load
V_{res}	The residual strength of RC frame and masonry infill
R_{res}	The story drift at point of V_{res}

1 Introduction

Many RC buildings in the world use masonry infills as partition walls. The masonry infill is considered as a non-structural element but its influence on structural behaviour has been repeatedly been observed in recent earthquakes such as the 2009 L'Aquila earthquake in Italy, 2008 Sichuan earthquake in China, 1999 Izmit earthquake in Turkey, 2015 Nepal earthquake and the 2016 Ecuador earthquake.

The seismic performance of masonry infill depends on several parameters such as the confinement effect, masonry type, aspect ratio, mortar strength. Among these factors, the relative strength of the boundary RC frame to the masonry infill is a crucial parameter that not only governs the behaviour and failure modes of the RC frame but also the strength and failure mode of the masonry infill. This was demonstrated in an experimental study

conducted by Mehrabi et al. (1996). A study by Wood (1978) emphasized the impact of frame to masonry infill strength ratio on failure mechanism and proposed empirical equations to calculate shear strength based on this ratio. However, in another proposed empirical equation by Mainstone (1971) which was also adopted by FEMA 306 (1998), greater emphasis was placed on the frame to infill stiffness ratio rather than strength in controlling the equivalent strut width which is used to calculate frame strength and initial stiffness. On the other hand, Liauw and Kwan (1985) proposed different diagonal compression failure modes of the infill based on plastic collapse theory. The proposed equations were directly related to the ratio of frame to masonry infill strength and the stiffness ratio was not taken into account. Saneinejad and Hobbs (1995) proposed analysis methods based on the contact length between the frame and masonry infill which was controlled by the ratio of frame strength to masonry infill strength. However, based on extensive experimental data, Flanagan and Bennett (1999) concluded that the strength of compression failure mechanism of the masonry infill was not significantly influenced by the frame to masonry infill strength or stiffness ratios and instead proposed simplified empirical equations which did not use either ratio. ASCE/SEI 41 (2007) proposed equations to calculate the masonry infill strength based on shear tests of masonry infill ignoring the frame to masonry infill strength ratio. However, the strength ratio was used to determine deformation limits for the masonry infill. Turgay et al. (2014) conducted a comparative study between different codes to estimate strength, deformation and stiffness of masonry infill. The comparative study showed large variation in the commonly used analytical models to calculate strength and stiffness. Turgay et al.'s study also showed that deformation limits suggested by ASCE 41 based on the frame to infill strength ratio was overly conservative. In summary, the experimental results and equations proposed by various researchers tend to contradict each other. Some studies placed emphasis on the importance of the frame to infill strength ratio while others emphasized the importance of the frame to infill stiffness ratio and others ignored the influence of these ratios altogether.

In addition, the large variation in analytical models proposed by codes or researchers to estimate the seismic capacity of masonry infills can create complications and confusion for practicing engineers during design. Many engineers still assume that the walls are non-structural elements due to variations in estimating seismic capacity concerning RC frames with masonry infill behaviour and the complexity in evaluating their failure modes.

Therefore, this study aims to clarifying the impact of frame strength on the seismic capacity of masonry infill. The influence of frame to infill strength and stiffness ratios on the strength, stiffness and deformation limits is investigated. In the first part of this study, two ½ scale specimens with different RC frames and identical masonry infill walls were tested using a static cyclic loading protocol. In the second part of this study, an investigation was conducted on the deformation limits of masonry infilled RC walls and the influence of various parameters, based on data collected from many recent experimental tests. Finally, a simplified procedure was proposed based on experimental data that can estimate the backbone curve and provided a good estimate of the post-peak lateral strength degradation slope based on the frame to infill strength ratio using simple hand calculation. This simplified method can aid practicing engineers to better understand the expected behaviour of masonry infilled RC frames during preliminary design.

2 Experimental program

2.1 Test specimens

Two half-scaled specimens with different RC frames, having same unreinforced masonry infills, were designed. The main variance parameter for test specimens was the ratio of the boundary frame to masonry infill lateral strength defined as β index, as shown in Eq. (1). Specimens named WF (weak frame) and SF (strong frame) with β of 0.4 and 1.5, respectively.

$$\beta = V_f / V_{\text{inf}} \tag{1}$$

where V_f is the boundary frame lateral strength which is calculated to be the ultimate flexural capacity of a bare frame with plastic hinges at top and bottom of columns. The V_{inf} is the masonry infill lateral strength calculated based on Eq. (2) which is a simplified empirical equation showing good agreement with experimental database studied by the author (Al-Washali et al. 2017)

$$V_{\text{inf}} = 0.05 f_m \cdot t_{\text{inf}} \cdot l_{\text{inf}} \tag{2}$$

where f_m is the compressive strength of masonry prism, t_{inf} is the infill thickness, l_{inf} is the infill length.

The specimen dimensions and details are shown in Fig. 1. Both specimens were identical except for the column size and reinforcement, as shown in Fig. 1. The beams

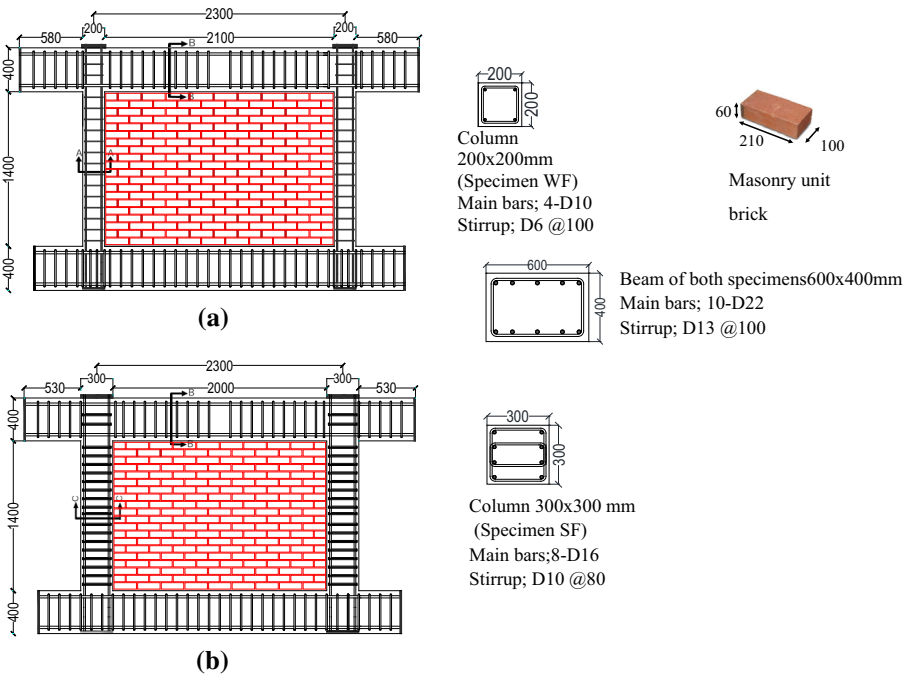

Fig. 1 Dimensions and reinforcement of specimens; units in mm. **a** Specimen WF (weak frame), **b** specimen SF (strong frame)

were designed to be stronger and stiff enough to simulate a typical case of a weak column and strong beam system observed in existing buildings of old designs.

2.2 Material properties

The infill panels were constructed using 60 × 100 × 210 mm solid clay bricks conventionally used in Japan. It should be noted that masonry infills are not commonly used in Japan, but the purpose of the study is to investigate the influence of changing the strength of boundary frame on the masonry infill that are used around the world as general case. A professional mason built the infill, after the frame construction, where its thickness is 100 mm and mortar head and bed joint thickness is about 10 mm. Tables 1 and 2 show the properties based on material tests conducted on the reinforcing steel, concrete and masonry respectively, where those values represent the mean values of three samples in each test. These include steel tensile strength by JIS Z 2201 (2010), the compression strength of concrete and mortar cylinders by JIS A 1108 (2010), the splitting tensile strength of concrete and mortar cylinders by JIS A 1113 (2010), the masonry prism compressive strength tested according to ASTM C1314 (2011). The concrete used for both specimens was identical and from the same batch. The proportion of cement and sand for the mortar is 1:2.5 (mass proportion), and masonry prism samples were made simultaneously with the infill panel by the same professional mason. The material tests were conducted at the same time with the experimental loading for each specimen individually. There is an increase of compressive strength of concrete, mortar and masonry prism strength in both specimens and this is considered to be caused by the time gap between material tests (3 weeks difference in both specimens).

2.3 Test setup and instrumentation

The loading system is shown schematically in Figs. 2 and 3. The vertical load was applied on RC columns by two vertical hydraulic jacks and was maintained to be 200 kN on each column. Two pantograph, attached with the vertical jacks, restricted any torsional and out-of-plane displacement. Two horizontal jacks, applying together an incremental cyclic loading, were attached at the beam level and were controlled by a drift angle of R%, defined as the ratio of lateral story deformation to the story height measured at the middle depth of the beam ($h = 1600$ mm). The lateral loading program consisted of 2 cycles for each peak drift angle of 0.05, 0.1, 0.2, 0.4, 0.6, 0.8, 1, 1.5 and 2%.

2.4 Experimental results

The lateral load versus story drift angle graphs of both specimens are shown in Figs. 4 and 5. Hinge locations during positive loading are schematically shown Fig. 6. Cracks and failure patterns at story drift of 0.8% and final drift cycle of 2.0% are shown in Fig. 7.

2.4.1 For specimen WF

Very small cracks on mortar bed joint and diagonal cracks on bricks near loading corner of infill panel, less than 0.3 mm width, started at early stages of loading just when the drift angle was 0.05%. At drift angles of 0.2 and 0.4%, the longitudinal reinforcement in the tensile column (windward column) yielded at the upper critical section and above its mid-

Table 1 Material properties of concrete and masonry details

Specimen name	Frame concrete			Masonry prism			Mortar cylinders compressive strength (MPa)	Brick unit compressive strength (MPa)
	Compressive strength (MPa)	Elastic modulus (MPa)	Split tensile strength (MPa)	Compressive strength (MPa)	Elastic modulus (MPa)	Strain at peak stress		
WF	24.2	2.3×10^4	2.1	17.3	7840	0.0037	20.2	38.1
SF	28.3	2.3×10^4	2.4	18.6	8140	0.0039	29.2	38.1

Table 2 Reinforcement mechanical properties

Bar	Nominal strength	Yield strength (MPa)	Ultimate tensile strength (MPa)
D6	SD345	476	595
D10	SD345	384	547
D13	SD345	356	555
D16	SD345	370	556
D22	SD390	447	619

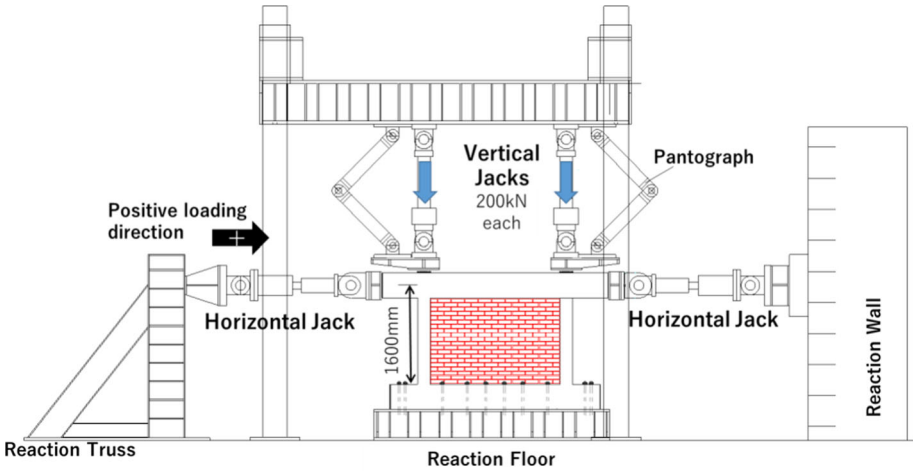

Fig. 2 Test setup (units: mm)

height, respectively, forming failure mechanism similar to a short column, as illustrated in Fig. 6a. The yielding of columns was detected using strain gauges attached on the main reinforcing bars of columns at critical sections and distributed uniformly every 200 mm over the height of the columns. Just after reaching the maximum lateral strength, there was a sudden drop of lateral load bearing capacity with extensive cracking and spalling of bricks. After the drift of 1%, the main failure mechanism changed from diagonal cracks to sliding cracks with clear sliding movement at the mid-height of the infill. At drift story of 2% in the negative cycle, the concrete around the reinforcement of top compression column spalled-off and main bars buckled.

2.4.2 For specimen SF

Cracking of infill panel also started at the peak of the first loading cycle, which was relatively similar to the crack width observed in specimen WF at this stage. At drift angle between 0.6 and 0.7%, both columns yielded at the locations shown in Fig. 6b. As it reached its maximum strength, the lateral load gradually degraded (contrarily to the sudden degradation of strength in previous specimen WF) with the drift angle increase until the drift angle of 1.5%, where there was a slight drop of the lateral load, after the horizontal sliding between bricks clearly increased. At the drift angle of 2%, the loading stopped as

Fig. 3 Photo of test setup

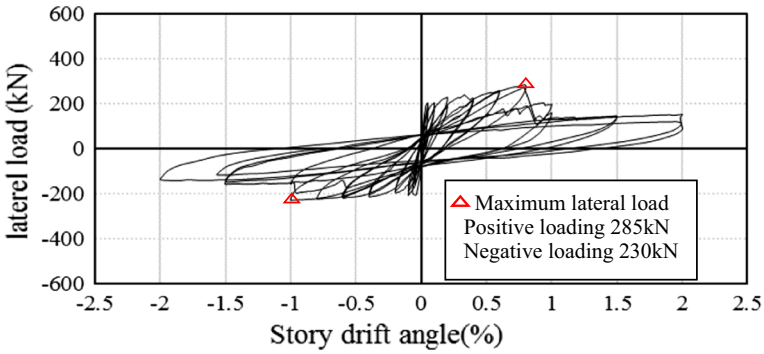

Fig. 4 Lateral strength and story drift angle for specimen WF

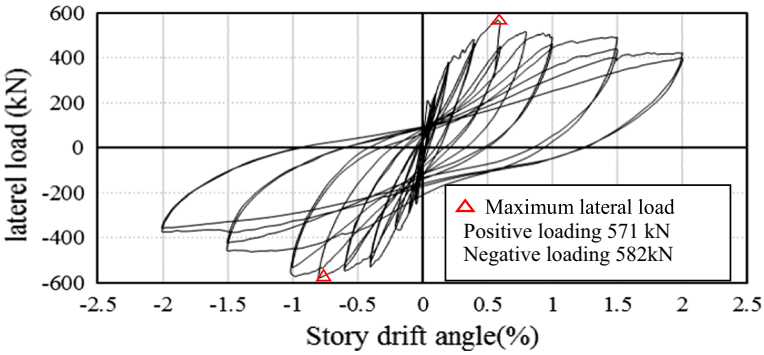

Fig. 5 Lateral strength and story drift angle for specimen SF

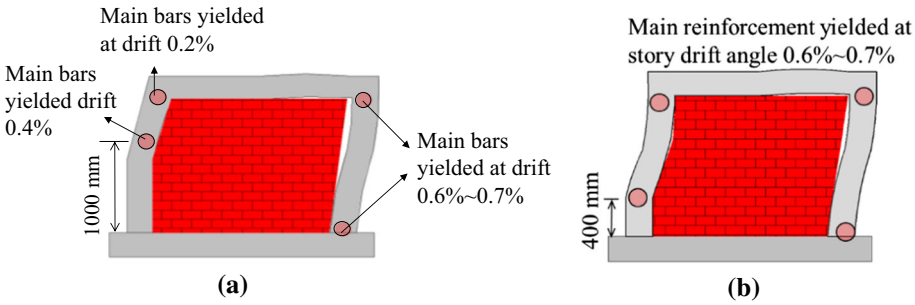

Fig. 6 Hinge locations formed in RC frame. **a** Specimen WF, **b** specimen SF

planned, and the masonry infill damage at this point was much greater than observed in the previous specimen WF (see Fig. 6b). In spite that columns had many cracks, there was no extensive damage or spalling of concrete cover.

3 Discussion of experimental results

3.1 Lateral strength

The maximum lateral load contributed by the masonry infill (V_{inf}) is calculated by deducting the bare frame lateral strength (V_f) from the maximum lateral load of the overall structure (V_{max}), as shown in Eq. (4). It should be noted that obtaining the actual maximum lateral strength of the infill can be more complicated due to the complicated frame-panel interaction, variation of hinge locations and internal varying axial load on columns, which are very challenging to pre-identify. Therefore, in order to make more general seismic evaluation possible and as comparison benchmark, Eq. (4) was employed in this study.

$$V_f = 4M_u/h_o \tag{3}$$

$$V_{\text{inf}} = V_{\text{max}} - V_f \tag{4}$$

where M_u is the minimum plastic moment of the column or beam calculated by AIJ provision (2016) and h_o is the clear height of column (taken here as infill height). The moment capacity of column ends was calculated using axial load (200 kN) applied by vertical jacks.

Table 3 shows the experimental shear strength of masonry infills in both specimens, which is the shear force (V_{inf}) divided by the infill cross-sectional area. Even though both infill panels were made by exactly same material and have similar prism compression strength, specimen SF has the shear capacity of 1.48 N/mm^2 which is about 1.5 times the shear strength in specimen WF (0.93 N/mm^2).

The large increase in shear strength is thought to be mainly due to confinement effect of the strong boundary frame in specimen SF. It is thought that the stronger and stiffer boundary RC frame will result in increase of the contact length between frame and masonry infill. Thus, the increase of the infill's compression strut width increased the lateral strength capacity. The mortar strength of specimen SF was higher than that of specimen WF, as mentioned earlier in Table 1, so it might affect the failure pattern and lateral strength of infill. However, the prism strength of the infill is the most crucial factor

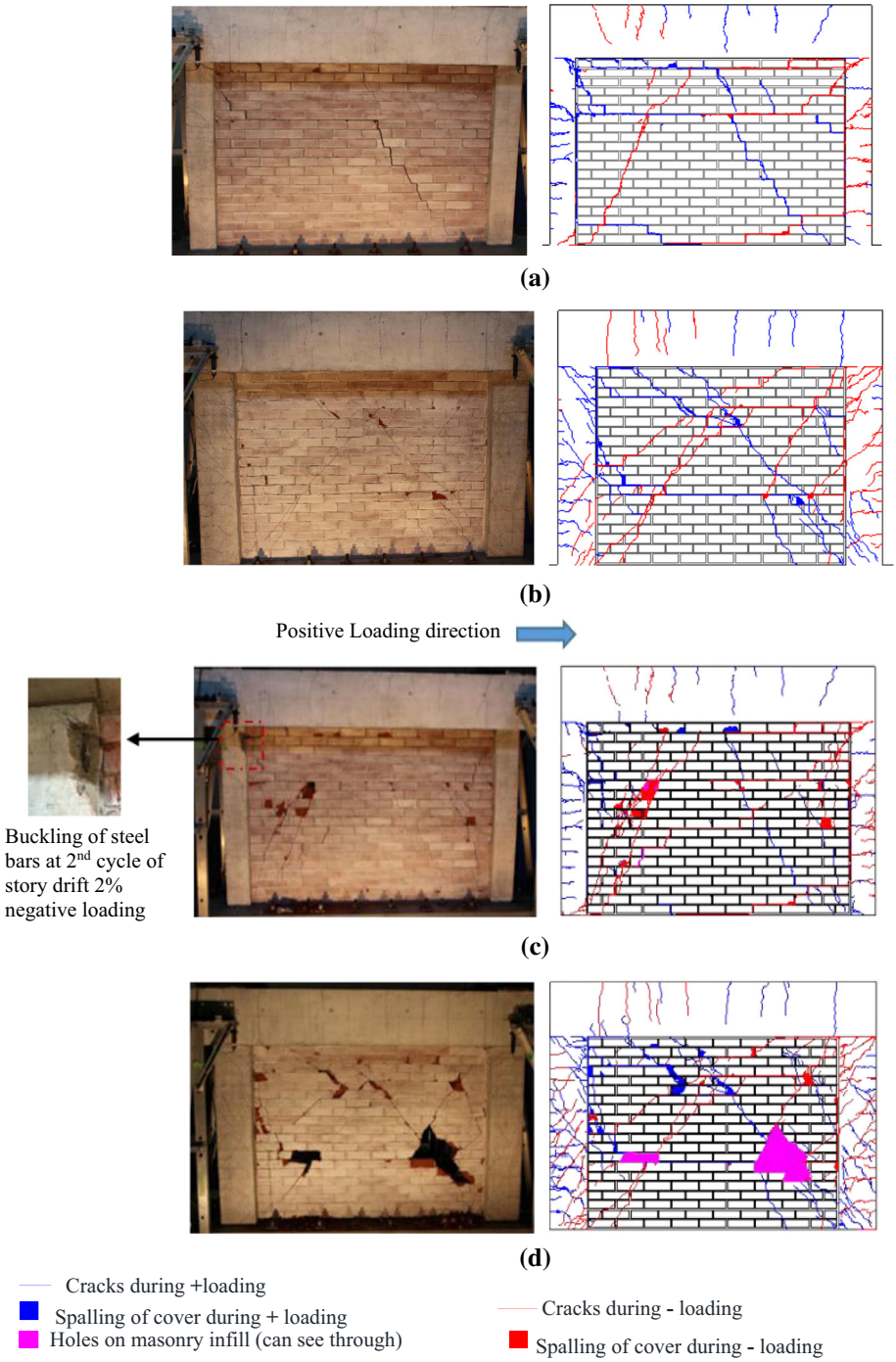

Fig. 7 Crack patterns observed at story drift of 0.8 and 2% for both specimens. **a** Specimen WF at story drift 0.8%, **b** specimen SF at story drift 0.8%, **c** specimen WF at story drift 2%, **d** specimen SF at story drift 2%

Table 3 Maximum lateral load and shear strength of infill

Specimen name	Experiment V_{max} (kN)		V_f (kN) Eq. (3)	Experiment V_{inf} (kN) by Eq. (4)		Maximum shear strength τ_{inf} (N/mm^2)		Average V_{inf} of both directions (kN)	Average shear strength τ_{inf} of both directions (N/mm^2)
	Positive loading	Negative loading		Positive loading	Negative loading	Positive loading	Negative loading		
WF	285	230	71	214	159	1.07	0.80	186.5	0.93
SF	571	582	280	291	302	1.46	1.51	296.5	1.48

to determine the main failure mechanism and lateral strength from many researches. Thus, the difference in lateral strength between specimens SF and WF are considered mainly due to different boundary RC frames.

The in-plane capacity of the masonry infill depends mainly on the type of failure mechanism. The failure mechanism types and identification are different between building standards or researchers. The most recognized failure modes are diagonal compression failure and sliding shear failure modes. The failure mechanism observed in experimental results as mentioned earlier, is a mixture of both: compression and sliding failure.

Several common strength calculation methods for both diagonal compression and sliding failure modes, which were cited by many researchers, will be introduced and compared to the experimental results.

3.1.1 For diagonal compression failure mode

FEMA 306 (1998) adopted a modified version of the method suggested by Stafford-Smith to calculate the compression failure by the equivalent diagonal strut. The shear force (horizontal component of the diagonal strut capacity) is calculated from Eqs. (5) through (7);

$$V_{\inf} = W_{ef} \cdot t_{\inf} \cdot f_{m90} \cdot \cos\theta \tag{5}$$

$$W_{ef} = 0.175.\,(\lambda_h H)^{-0.4} \cdot d_m \tag{6}$$

$$\lambda_h = \left[\frac{E_w t_w \sin(2\theta)}{4E_c I_c H_{\inf}}\right]^{\frac{1}{4}} \tag{7}$$

where W_{ef} is the equivalent strut width calculated using Eq. (6), t_{inf} is the infill thickness, E_w and E_c are the elasticity moduli of the infill wall and the concrete. H_{inf} and H are the net height of infill wall and the story height. θ *is* the arctan (H_{inf}/L_{inf}) (the inclination of the diagonal). I_c is the moment of inertia of the column, d_m is diagonal length of masonry infill, f_{m90} is the expected prism compressive strength of masonry in horizontal direction, which may be set at 50% of the expected prism compressive strength in absence of experimental results.

Liauw and Kwan (1985) used plastic collapse theory and proposed different diagonal compression failure modes of the infill, and the minimum value stated in Eqs. (8) through (10) is the expected in-plane strength. This method not only estimates the masonry infill strength but also calculate the in-plane strength of the whole system consisted of RC frame and masonry infill.

$$V_1 = f_m \cdot t_{\inf} \cdot h_{\inf}\sqrt{2(M_{pj} + M_{pc})/(f_m \cdot t_{\inf} \cdot h^2)} \tag{8}$$

$$V_2 = (f_m \cdot t_{\inf} \cdot h_{\inf})/\tan\theta \cdot \sqrt{(2(M_{pj} + M_{pb})/(f_m \cdot t_{\inf} \cdot h_{\inf}^2)} \tag{9}$$

$$V_3 = f_m \cdot t_{\inf} \cdot h_{inf}/6 + 4M_{pj}/h_{\inf} \tag{10}$$

where M_{pc} is the plastic moment capacity of the column, M_{pb} is the plastic moment of the beam and M_{pj} is the minimum of M_{pb} and M_{pc}.

Flanagan and Bennett (1999) proposed the corner crushing infill strength as a simple form, as shown in Eq. (11), based on their experimental tests that stated a different conclusion from previous researchers, where the corner crushing capacity does not change because of frame properties and geometry.

$$V = K_{ult} \cdot t_{inf} \cdot f_m \tag{11}$$

where K_{ult} is an empirical value based on their experiments, and it is suggested to be 246 mm.

3.1.2 For sliding shear failure

FEMA 306 (1998) suggests that Mohr–Coulomb failure criteria can be used to assess the initial sliding shear capacity of the infill as shown in Eq. (12):

$$V = \tau_o \cdot t_{\inf} \cdot l_{\inf} + \mu \cdot N \tag{12}$$

where μ is the coefficient of sliding friction along the bed joint, FEMA 306 (1998) does not suggest any values for μ. However, the New Zealand Society for Earthquake Engineering, NZSEE (2006) which uses the same procedure as FEMA 306 suggests $\mu = 0.8$, in the absence of such site specific data. N is vertical load on the infill wall and τ_o is the cohesive capacity of the mortar bed joint which can be taken as Eq. (13). In this study, the panels were inserted after construction of the frame and the vertical load by jacks were then applied on the columns. In addition, there was no additional axial loading applied on the beam. Therefore, vertical gravity load N was considered very small and taken as zero in Eq. (12).

$$\tau_o = f_{m90}/20 \tag{13}$$

where f_{m90} is the expected strength of masonry in horizontal direction, which may be set at 50% of the expected prism compressive strength.

Paulay and Priestley (1992) also employed the Mohr–Coulomb failure concept to assess the sliding shear capacity. They assumed that the vertical component of the strut compression force acts as vertical load on the infill. It is suggested that maximum sliding shear force of masonry infill as Eq. (14).

Table 4 Ratio of experimental peak strength to analytical results

Test specimen	FEMA 306 (1998) (compression failure)	Liauw and Kwan (1985)	Flanagan and Bennett (1999)	FEMA 306 (1998) (Sliding failure)	Paulay and Priestley (1992) (Sliding failure)	Al-Washali et al. (2017)
Specimen WF	1.21	0.69	0.50	3.14	1.58	1.18
Specimen SF	1.41	0.81	0.66	6.26	2.13	1.62
Average	1.31	0.75	0.58	4.70	1.85	1.40

Ratio = experimental/analytical

$$V = (\tau_o \cdot t_{\text{inf}} \cdot l_{\text{inf}})/((1 - \mu \cdot (h/l))) \tag{14}$$

where Paulay and Priestley (1992) recommended values of $\tau_o = 0.03f_m$ and $\mu = 0.3$.

Table 4 shows the comparison of the infill strength with previously mentioned methods. Liauw and Kwan (1985) method and simplified method of Flanagan and Bennett (1999) greatly overestimate the strength. The methods proposed to calculate sliding capacity by FEMA 306 (1998), and Paulay and Priestley (1992) greatly underestimated the infill strength. Diagonal compression strength by FEMA 306 (1998) and the simplified equation by Al-Washali et al. (2017) showed relatively good estimation for specimen WF, but they highly underestimated that of Specimen SF. This underestimation is considered due to the ignorance of the confinement effect by the strong boundary frame in their equations.

3.2 Stiffness

The initial stiffness K_o of infilled frame is taken as the slope between the origin point of the load–displacement curve and the point at which there is a major visible crack in the masonry infill and the RC frame, which was determined to occur at story drift of 0.1%. Table 5 shows the comparison between the initial stiffness of overall frames and that of bare frames. Herein, the initial stiffness of bare frame is calculated based on its elastic gross concrete section. The masonry infill greatly increased the initial stiffness up to about 7.1 times that of bare frame in specimen WF. Therefore, in seismic design, ignoring the contribution of masonry infill to stiffness and natural period of building may cause non-conservative design practice, since buildings with lower natural period have greater seismic forces.

The most well recognized method for calculating the infill stiffness is using the equivalent diagonal compression strut, which has the same elasticity and thickness as the infill panel. Paulay and Priestley (1992) recommended using the effective width of strut (W_{ef}) as 0.25 times the diagonal length of infill panel (d_m), as shown in Eq. (15).

$$W_{ef} = 0.25\, d_m \tag{15}$$

Table 5 shows the comparison between experimental and numerical initial stiffness based on the strut width recommended by FEMA 306 (1998) and Paulay and Priestley (1992), where the vales include the initial stiffness of bare frames. The strut width calculated by FEMA 306 (1998) underestimates the initial stiffness by about 1.9 and 1.08 for specimens WF and SF, respectively. On the other hand, Eq. (15) recommended by Paulay and Priestley (1992) agrees pretty well with specimen WF with the ratio of 0.94, but highly overestimates specimen SF with the ratio of 0.73. Based on test results, it was found that making a simple assumption of the strut width W_{ef} to be 0.2 d_m (d_m: diagonal length), which is a slightly modified assumption from Paulay and Priestley (1992), gives relatively better and conservative estimate for the initial stiffness. The strut width using FEMA 306 (1998) commonly gives the strut width of 0.08–0.15 d_m based on relative stiffness between RC frame and masonry infill, with the average of about 0.1 d_m for many experimental studies presented later in this paper. The assumed strut width in this study of 0.2 d_m is somewhere in between FEMA 306 and Paulay and Priestley (1992) equations. This estimation also showed reasonable agreement not only for the two tests in this study but also good agreement with other test data which will discussed later in this study.

Table 5 Comparison of analytical and experimental initial stiffness

Specimen	Exp. stiffness Initial stiffness (kN/mm)	Calculated stiffness							
		Bare frame		Initial stiffness using diagonal strut model (including bare frame)					
		Initial stiffness (kN/mm)	Ratio	FEMA 306 (1998) (kN/mm)	Ratio	Paulay and Priestley (1992) (kN/mm) $W_{ef} = 0.25\ d_m$	Ratio	This study $W_{ef} = 0.2\ d_m$	Ratio
WF	128	18	7.07	68	1.90	136	0.94	114	1.13
SF	150	79	1.91	139	1.08	205	0.73	180	0.84
Average		4.49		1.49		0.84		0.94	

Ratio = experimental/analytical

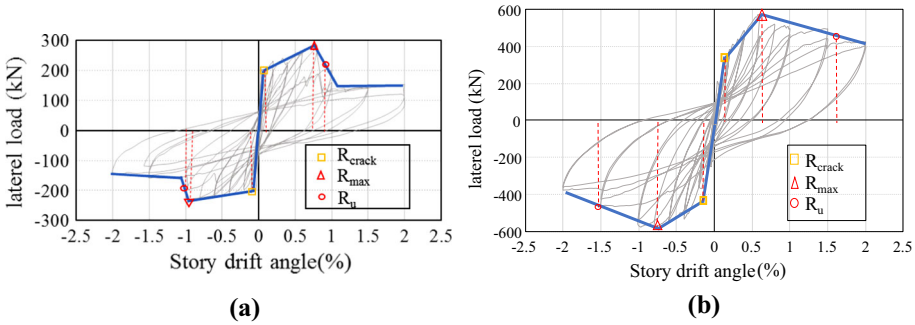

Fig. 8 Backbone curve and deformation limits. **a** Specimen WF, **b** specimen SF

3.3 Deformation

In this study, idealized backbone curves for specimen WF and SF are shown in Fig. 8. Herein, R_{crack}, R_{max} and R_u are the representative drift angles at the cracking, the maximum strength and the strength degradation point, respectively. Strength degradation point R_u is set to be 80% of the maximum strength. It should be noted that R_u does not indicate the safety deformation limit, but used herein for comparison benchmark, since it is used for many other literature such as Mehrabi et al. (1996) and Turgay et al. (2014).

R_{crack} and R_{max} are estimated to be 0.1 and 0.8% for both specimens. R_u was found to be 0.9 and 1.6% for specimens WF and SF, respectively. Therefore, it was concluded that the influence of surrounding frame strength on R_{crack} and R_{max} was slight, but it greatly alters the strength degradation slope. The smooth decrease of strength and improvement of ductility for specimen SF are considered to be due to the confinement by the stronger surrounding frame, which reduces the inelastic deformation of masonry infill.

4 Investigation of deformation of masonry infilled RC frames from past literature

Due to the many parameters and variability of masonry infill materials around the world, the deformation drift of R_{crack}, R_{max} *and* R_u are in large ranges and past experimental studies are of considerable differences from each other. As for standards, the FEMA 306 (1998) states that cracking begins at inter-story drifts of 0.25% and is completed by about 0.5%. ASCE41/SEI (2007) defines the inter-story drift limit, where the strength significantly drops, as a function using the ratio of the frame shear strength over that of the infill, β, and the aspect ratio, L_{inf}/h_{inf}, and the drift ranges between 0.3 and 1.5%. Recently, Turgay et al. (2014) checked the ASCE41/SEI (2007) method using β index and aspect ratio with approximately 50 frame test results. The results of the study showed that ASCE41 might be over conservative in most cases.

Masonry infills are made of many different materials and characteristics which greatly influence its deformation limits. However, the material characteristics in the aforementioned studies are not addressed in estimating the deformation limits. In this paper, in addition to the β index and aspect ratio, the deformation limits are studied based on several recent experimental studies with two additional important parameters: compressive strength and Young's modulus of elasticity of masonry prism. The objective of this part is

to find a general simplified way to estimate the drift limits of the backbone curve of RC frames with masonry infill based on the results and analysis of many different experiments conducted around the world and identify the several parameters influencing deformation capacity. The scope of this study concerned with masonry infill without opening and that masonry infill is attached to the surrounding RC frame.

4.1 Outline of the experiments database

The database consisted of 24 of 1 span, 1 story RC frames with masonry infill tested under static loading from 9 researchers: Mehrabi et al. (1996), Jin et al. (2016), Suzuki et al. (2017), Kakaletsis and Karayannis (2009), Blackard et al. (2009), Al-Nimry (2014), Imran and Aryanto (2009), Bose and Rai (2016) and Maidiawati and Sanada (2017) are shown in Table 6. The data chosen consist of different types of masonry infill to represent a general case for different masonry types used in the world. The data chosen are of a single span with unreinforced masonry infill without opening or retrofit.

4.2 Parameters influencing deformation R_{max} and R_u

Based on the studied experiments, the R_{max} drift has an average of 0.73% and most of values in the range of 0.4–0.9%. The R_u drift angle has an average of 1.72%, but a standard deviation of 0.72, which means values are of a wide range.

The deformation drift R_{max} and R_u of masonry infilled RC frames are investigated based on the influence of the following parameters: compressive strength f_m and young modulus elasticity of masonry infill E_m, aspect ratio L/H and ratio of expected frame strength to expected infill strength (β), in Figs. 9, 10, 11 and 12 respectively. It should be noted that in the absence of masonry infill young modulus elasticity in experimental data, it was estimated from the recommendation by Paulay and Priestley (1992), where $E_m = 700\, f_m$.

The lower the masonry infill compressive strength and its elasticity, the greater the tendency of having larger R_{max} and R_u, as shown in Figs. 9 and 10. On the other hand, the aspect ratio relation with deformation drift R_{max} and R_u are not clear in the studied experimental data as shown in Fig. 11. It should be noted that the aspect ratio investigated are of a narrow range of 1–2 because of a limited experimental data outside these ranges. The ratio of frame strength to masonry frame shear strength, β, has directly proportional relation with deformation limits R_u as shown in Fig. 12b. Comparison with the standard ASCE41/SEI (2007) in Fig. 12b shows that the ASCE41/SEI (2007) limits are in the safe side but overly conservative.

4.3 A simplified procedure to estimate the backbone curve of infilled RC frames

Sophisticated methods using FEM or similar micro models that are simulated based on the experimental data need a huge computational effort with many detailed experimental material characteristics that are unknown in design by practicing engineers. Thus, simplified procedure is proposed that can apply to general types of masonry infill with limited amount of material data, based on the investigation on stiffness, strength and deformation limits of the experimental study presented earlier. The procedure is meant to be as easy as possible so that it can be used in preliminary design process even with simple hand

Table 6 Investigated past experimental data and deformation limit R_{max} and R_u

Name of researcher	Specimen name	Type of Infill	L/H ratio	f_m (MPa)	Experimental max lateral load (kN)	R_{max} (%)	R_u(%)	β
Mehrabi et al. (1996)	3	Solid bricks	1.50	15.1	278	0.4	1.16	0.64
	4	Hollow bricks	1.50	10.6	162	0.63	1.45	0.82
	5	Solid bricks	1.50	13.8	267	0.79	1.42	0.62
	6	Hollow bricks	1.50	10.1	207	0.6	1.8	1.40
	7	Solid bricks	1.50	13.6	490	0.7	1.0	1.05
	8	Hollow bricks	1.50	9.5	190	0.9	1.8	0.92
	9	Solid bricks	1.50	14.2	293	0.5	2.0	0.62
	10	Hollow bricks	2.07	10.6	190	0.4	1.9	0.60
	11	Solid bricks	2.07	11.4	293	0.7	1.5	0.55
	12	Solid bricks	2.07	13.6	363	0.6	1.0	0.47
Jin et al. (2016)	IFRB	Concrete block	1.46	6.7	61	0.4	1.5	2.24
	IFFB	Concrete block	1.46	6.7	50	0.4	2.0	1.96
Suzuki et al. (2017)	1S-1B	Concrete block	1.65	8.4	59	1.0	2.0	0.96
	1S-1B-V	Concrete block	1.65	3.6	50	1.5	2.8	2.25
Kakaletsis and Karayannis (2009)	S	Hollow bricks	1.50	5.1	82	0.9	2.3	2.02
Blackard et al. (2009)	S	Brick * double wythe	1.81	19.1	681	0.3	0.6	0.16
Al-Nimry (2014)	IF4	Stone and concrete	1.17	16.6	169	0.4	1.1	0.27
	IF5	Stone and concrete	1.17	16.6	165	0.4	0.9	0.23
Imran and Aryanto (2009)	Model 1	AAC blocks	1.00	3.0	111	0.9	2.9	2.13
	Model 2	Brick	1.00	3.7	106	1.2	3.0	1.70
Bose and Rai (2016)	IF-AAC	AAC blocks	1.65	2.4	146	1.9	3.7	2.57
Maidiawati and Sanada (2017)	IF-SBw/FM	Brick	16.3	16.3	175	0.5	1.0	0.77
This study	WF	Brick	1.50	17.3	285	0.8	0.9	0.39
This study	SF	Brick	1.43	18.6	582	0.8	1.5	1.51
Average						0.73	1.72	
Standard deviation						0.39	0.78	

calculation. The scope of this simplified procedure is unreinforced masonry infill with no openings and almost no construction gaps between frame and infill panel.

The simplified procedure is based on the following assumptions:

a) The backbone curve for RC frame is modeled by bi-linear as shown in Fig. 13a. The initial stiffness of frame K_f is calculated by theoretical equations proposed by Chopra

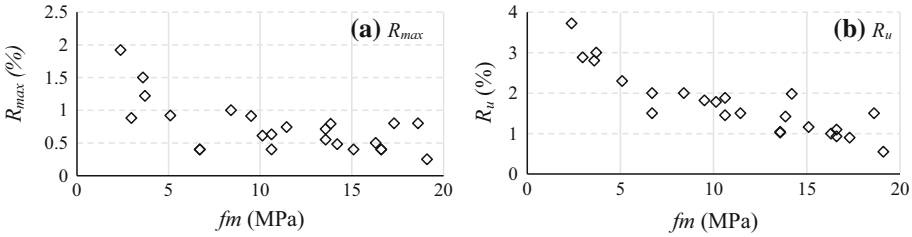

Fig. 9 Relationship of masonry prism compressive strength f_m with of deformation limits

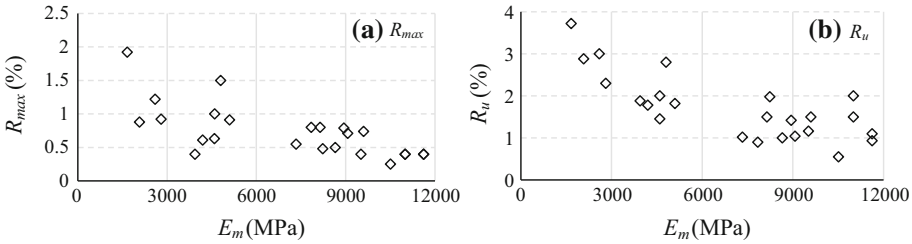

Fig. 10 Relationship of elasticity of masonry infill E_m with of deformation limits

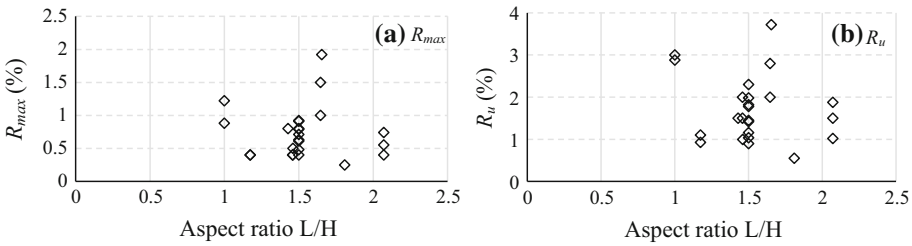

Fig. 11 Relationship of Aspect ratio *L/H* with of deformation limits

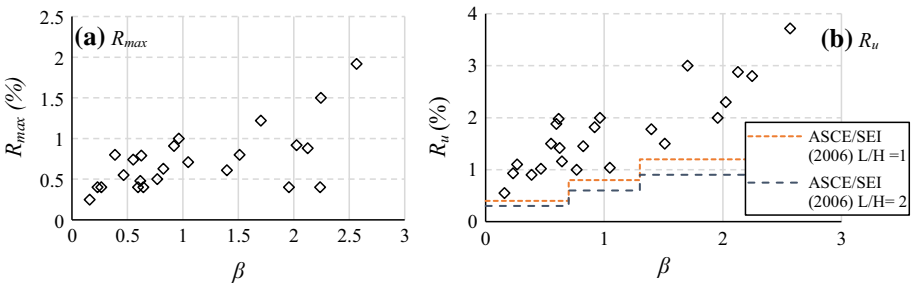

Fig. 12 Relationship of β and comparison with ASCE/SEI (2007) with deformation limits

(2007) for elastic stiffness of bare frame as shown in Eq. (16). For RC frames, the stiffness degrades after the cracking development. However, RC columns with URM infills are likely to behave as short columns in many cases, and the RC frame tends to act much stiffer than a bare frame. In this study, therefore, the skeleton curve for RC

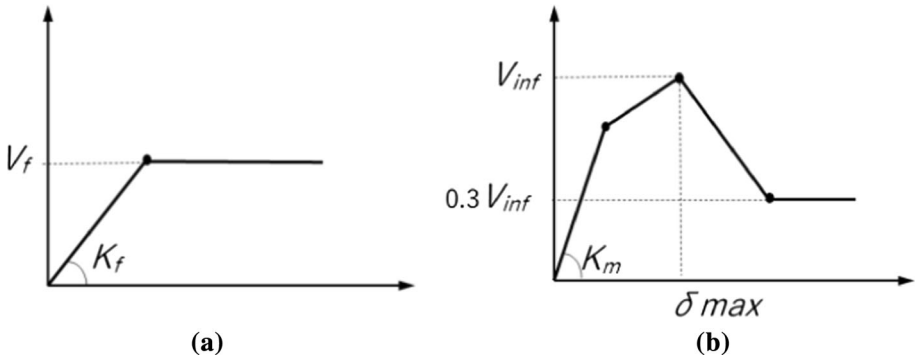

Fig. 13 Assumption of force versus drift curve. **a** Boundary frame, **b** infill wall

frame with URM infill was modeled as bi-linear for the simplicity for practical calculation as well as to reflect such behavior.

$$K_f = \left(\frac{24EI_c}{hc^3} \cdot \frac{12\rho + 1}{12\rho + 4}\right) \tag{16}$$

$$\rho = \frac{\sum EI_b/l_b}{\sum EI_c/h_c} \tag{17}$$

b) The backbone curve for masonry infill is shown in Fig. 13b. Herein, the lateral initial stiffness K_m, is converted from the axial stiffness of equivalent diagonal strut, as in Eq. (18):

$$K_m = \frac{E_m \cdot W_{ef} \cdot t_{\inf} \cdot \cos^2\theta}{d_m} \tag{18}$$

The effective width of strut, W_{ef}, is taken as 0.2 d_m which is a slightly modified assumption from Paulay and Priestley (1992) that showed good agreement with the experimental results mentioned previously. θ *is* the arctan (H_{inf}/L_{inf}) (the inclination of the diagonal).

c) The combination of backbone curve of frame and masonry infill shown in Fig. 13 will compose the backbone curve of the total system of infilled RC frames with 3 main

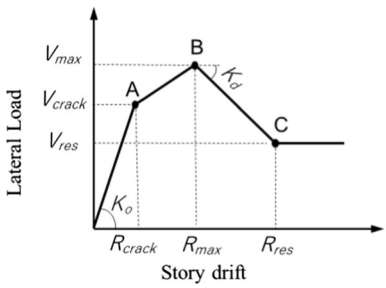

Fig. 14 Simplified backbone curve of masonry infilled RC frames

Table 7 Calculation summary of the simplified procedure

Points A, B and C (shown in Fig. 12)	Lateral strength	Story drift
Cracking point A	$0.7V_{max}$	$R_{crack} = 0.7V\max/K_o$ $(K_o = K_f + K_m)$ $K_f = \left(\frac{12EI_c}{h_c^3} \cdot \frac{12\rho+1}{12\rho+4}\right)$, $K_m = \frac{E_m \cdot W_{ef} \cdot t_{\inf} \cdot \cos^2\theta}{d_m}$ $W_{ef} = 0.2\ d_m$, *for initial stiffness* K_m
Maximum point B	$V_{max} = V_f + V_{inf}$	$R_{\max} = (\varepsilon_{peak} \cdot d_m)/\cos\theta$
Residual point C	$V_{res} = V_f + 0.3V_{inf}$	$R_{res} = R_{\max} + (V_{\max} - V_{res})/K_d$ $K_d = \eta \cdot K_m$, $\eta = 0.08/\beta^{0.75}$

points: Crack point, Max point and residual point named A, B, C, respectively as shown in Fig. 14.

d) Initial stiffness of masonry infilled RC frame, K_o, is calculated as summation of initial frame stiffness (K_f) and initial stiffness of masonry infill (K_m).

e) The cracking lateral strength V_{crack} is taken as $0.7V_{max}$, which is based on observations and showed good agreement of 24 specimen experimental data mentioned previously on Table 6. It should be noted that in actual behavior, the strength contribution of masonry infill and frame might not be divided equally as 70% at this cracking point, but assuming 70% contribution in average for both members gives a simplified reasonable agreement.

f) The maximum lateral load of the overall structure V_{max}, for the case of 1 single span frame, is the summation of frame max lateral strength V_f and masonry infill V_{inf}. V_{inf} will be calculated by aforementioned Eq. (5) assuming diagonal compression failure proposed by FEMA 306 (1998), which showed relatively good estimation with some conservativeness.

g) The residual strength V_{res}, shown in Fig. 14 is calculated as the summation of frame max lateral strength V_f and masonry infill lateral strength. Herein, the final contribution by masonry infill is set to be $0.3V_{inf}$.

h) The lateral displacement at maximum lateral load δ_{max} for a masonry infill is converted from diagonal strut as it reaches its maximum axial strain capacity of masonry prism compressive test as in Eq. (19).

$$\delta_{\max} = (\varepsilon_{peak} \cdot d_m)/\cos\theta \tag{19}$$

where ε_{peak} is the masonry compression strain at maximum compression stress, which was taken from the prism compression test shown in Table 1. The ε_{peak} of masonry prism commonly ranges between 0.002 and 0.004. In the absence of data of ε_{peak}, it can be calculated from some empirical equations based on experimental study of Kaushik et al. (2007). Also, in the case of 1 single span frame, the story drift at maximum lateral for infilled frames, R_{max}, is taken as the same point of δ_{max}.

i) The degradation slope of masonry infilled RC frame (K_d) is proposed based on regression analysis of data obtained in the experimental studies mentioned previously in Table 6 and relations shown in Figs. 9b, 10b and 12b, as per the following Eq. (20):

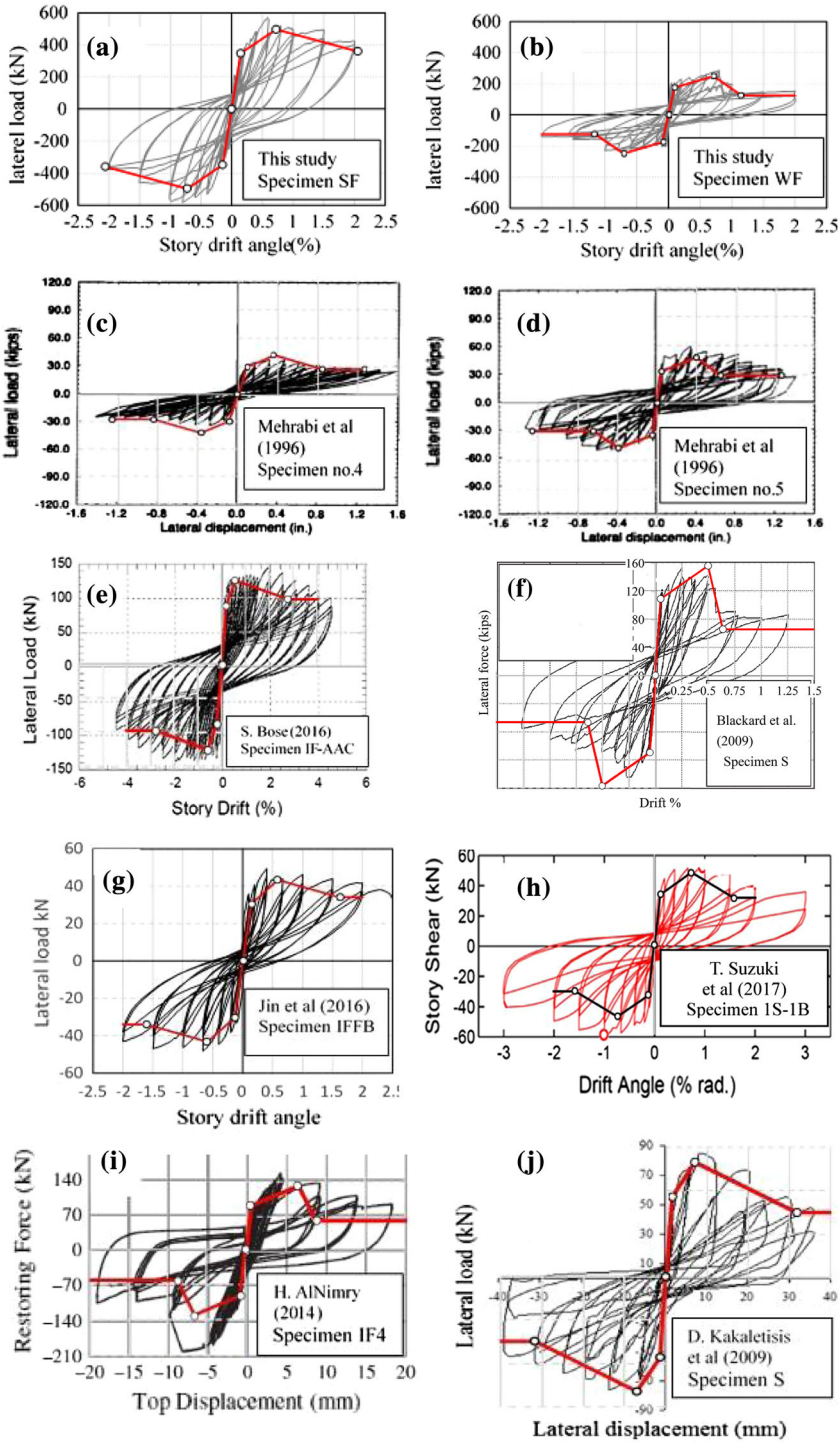

Fig. 15 Fitness of simplified procedure of backbone curve to experimental data (**a–i**)

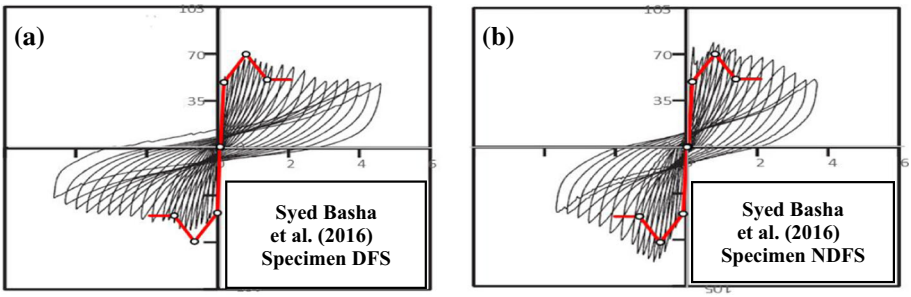

Fig. 16 Fitness of simplified backbone curve to experimental data not used in the calibration (**a**, **b**)

$$K_d = \eta \cdot K_m \tag{20}$$

$$\eta = 0.08/\beta^{0.75} \tag{21}$$

where η is an empirical index to account for the confinement by surrounding frame based on β.

It should be noted that aspect ratio influence is not included in the previous equations since it was difficult to find a clear reliable pattern as was shown in Fig. 11. The summary of the procedure is shown in Table 7.

5 Fitness of the simplified procedure

The proposed simplified analytical model for compressive stress–strain curves is examined for its fitness by comparing it with: experimental curves obtained in the present study and several past experimental data shown in Fig. 15. Figure 16 shows fitness of simplified backbone curve to experimental results by Syed Basha et al. (2016) that were not used for the calibration. The simplified procedure could well reproduce the major characteristic points on the backbone curve resulted from different sorts of masonry materials, and it showed good estimate of the general behavior of the curve with some conservativeness.

6 Conclusions

This paper presents the results of an experimental study as well as an investigation of experimental data presented in existing literature. The following major findings were obtained:

1. The experimental results showed that the shear strength of the masonry infill increased by up to 1.5 times when surrounded by a strong frame in comparison to a weaker frame (excluding frame shear strength). This result indicates that the strength of the masonry infill should not be calculated based solely on the results of masonry material testing due to the significant influence of the surrounding frame strength and stiffness.
2. The post peak degradation slope is much improved in the experimental results with increasing the ratio of frame shear strength to masonry infill. This parameter should be

taken into account in the design code of new RC buildings with masonry infill as it can change the brittle behaviour to be relatively more ductile.

3. The deformation limits of masonry infill are directly proportional to compressive prism strength of masonry and also to the RC frame to masonry infill shear strength ratio. However, the experimental data showed large variation about the influence of aspect ratio to deformation limits, which makes it difficult to conclude its influence based on the investigated experimental data. This point lacks experimental data and should be further investigated in future studies.
4. The authors' experimental results and the test results from existing literature are compared with predictions from available design guidelines. Although some recent design guidelines provide a safe value, they are overly conservative. Conversely, other recent researchers proposed methods may overestimate the masonry infill strength.
5. A simple procedure for the estimation of backbone curves of masonry infilled RC frames was proposed based on comparison of experimental results with existing literature. Such method is useful in preliminary design process by practical engineers to understand the general behaviour expected by infilled RC frames. In addition, the novelty of the proposed method is that it gives good estimation of the post-peak lateral strength degradation slope based on the ratio of frame to masonry infill strength which is not addressed in previous models. It should be noted that the simplified bi-linear frame model cannot represent the damage induced by rebar buckling and shear cracking. This is a limitation of the proposed backbone curve and needs further improvements in future studies.

Acknowledgements The study presented in this article was sponsored by the Science and Technology Research Partnership for Sustainable Development (SATREPS) project funded by JST (Japan Science and Technology Agency) and JICA (Japan International Cooperation Agency) for Bangladesh, 2015 project headed by Professor Nakano Yoshiaki, University of Tokyo and it's gratefully acknowledged. Opinions expressed in this article are those of the authors, and do not necessarily represent those of the SATREPS project.

References

Al-Nimry HS (2014) Quasi-static testing of RC infilled frames and confined stone-concrete bearing walls. J Earthq Eng 18:1–23

Al-Washali H, Suzuki Y, Maeda M (2017) Seismic evaluation of reinforced concrete buildings with masonry infill wall. In: The 16th world conference of earthquake engineering, Chile

American Society of Civil Engineers (ASCE) (2007) Seismic rehabilitation of existing buildings. Reston, Virginia (ASCE/SEI 41-06)

American Society of Testing and Materials (ASTM) (2011) Standard test method for compressive strength of masonry prisms. ASTM C1314, West Conshohocken, PA

Architectural Institute of Japan (AIJ) (2016) AIJ standard for lateral load-carrying capacity calculation of reinforced concrete structures (**in Japanese**)

Basha SH, Kaushi HB (2016) Behavior and failure mechanisms of masonry-infilled RC frames (in low-rise buildings) subject to lateral loading. J Eng Struct 111:233–245

Blackard B, Willam K, Mettupalayam S (2009) Experimental observations of masonry infilled RC frames with openings. ACI Special Publication, SP-265-9

Bose S, Rai DC (2016) Lateral load behavior of an open-ground-story RC building with AAC infills in upper stories. Earthq Spectra 32(3):1653–1674. doi:10.1193/121413EQS295M

Chopra Anil K (2007) Dynamics of structures, theory and application to earthquake engineering, 3rd edn. Pearson Prentice Hall, Upper-Saddle River

FEMA 306 (1998) Evaluation of earthquake damaged concrete and masonry wall buildings, Applied Technology Council (ATC-43 Project)

Flanagan RD, Bennett RM (1999) In-plane behavior of structural clay tile infilled frames. J Struct Eng 125(6):590–599

Imran L, Aryanto A (2009) Behavior of reinforced concrete frames in-filled with lightweight materials under seismic loads. Civil Eng Dimens 11(2):69–77

Japanese Industrial Standards (2010) Japanese Standards Association, No. JIS R1250, JIS Z 2201, JIS A 1108, JIS A 1113 (**in Japanese**)

Jin KW, Choi H, Nakano Y (2016) Experimental study on lateral strength evaluation of unreinforced masonry-infilled RC frame. Earthq Spectra 32:1725–1747. doi:10.1193/00714EQS152M

Kakaletsis DJ, Karayannis CG (2009) Experimental investigation of infilled reinforced concrete frames with openings. ACI Struct J 106(2):132–141

Kaushik HB, Rai DC, Jain SK (2007) Stress-strain characteristics of clay brick masonry under uniaxial compression. J Mater Civil Eng (ASCE) 19(9):728–739

Liauw TC, Kwan KH (1985) Unified Plastic analysis for infilled frames. J Struct Eng 111(7):1427–1448

Maidiawati, Sanada Y (2017) R/C frame–infill interaction model and its application to Indonesian buildings. Earthq Eng Struct Dyn 46(2):221–241

Mainstone RJ (1971) Summary of paper 7360: on the stiffness and strength of infilled frames. Proc Inst Civil Eng 49:230. doi:10.1680/iicep.1971.6267

Mehrabi AB, Shing PB, Schuller M, Noland J (1996) Experimental evaluation of masonry-infilled RC frames. J Struct Eng ASCE 122(3):228–237

New Zealand Society for Earthquake Engineering (NZSEE) (2006) Assessment and Improvement of the Structural Performance of Buildings in Earthquakes. NZSEE, Wellington, New Zealand, Section 9

Paulay, T. and Priestley, M.J.N. (1992) Seismic design of reinforced concrete and masonry buildings. Wiley, New York

Saneinejad A, Hobbs B (1995) Inelastic design of infilled frames. J Struct Eng 121(4):634–650

Suzuki T, Choi H, Sanada Y, Nakano Y, Matsukawa K, Paul D, Gülkan P, Binici B (2017) Experimental evaluation of the in-plane behavior of masonry wall infilled RC frames. Bull Earthq Eng. doi:10.1007/s10518-017-0139-1

Turgay T, Durmus MC, Binici B, Ozcebe G (2014) Evaluation of the predictive models for stiffness, strength, and deformation capacity of RC frames with masonry infill walls. J Struct Eng 140:06014003. doi:10.1061/(ASCE)ST.1943-541X.0001069

Wood RH (1978) Plasticity, composite action and collapse design of unreinforced shear wall panels in frames. Proc Inst Civil Eng Part 2 65:381–411